AAPS PharmSciTech, Vol. 13, No. 2, June 2012 (© 2012)
DOI: 10.1208/s12249-012-9791-6

Research Article

Ibuprofen-Loaded Calcium Stearate Pellets: Drying-Induced Variations in Dosage Form Properties

Simone Schrank,[1,2,3] Aden Hodzic,[3] Andreas Zimmer,[1] Benjamin J. Glasser,[4] Johannes Khinast,[2,3] and Eva Roblegg[1,3,5]

Received 11 January 2012; accepted 10 April 2012; published online 3 May 2012

Abstract. Pellets intended for oral dosing are frequently produced *via* extrusion/spheronization followed by drying. Typically, the last active process step, *i.e.*, drying, is assumed to have little effect on the final dosage form properties (*e.g.*, dissolution characteristics). Thus, there exist only a few studies of this subject. In the present study, calcium stearate/ibuprofen pellets were used as model system to investigate the impact of the drying conditions. Lipophilic calcium stearate matrix pellets containing 20% ibuprofen were prepared *via* wet extrusion/spheronization. Subsequently, desiccation, fluid-bed drying, and lyophilization were applied for granulation liquid removal. The impact of these drying techniques on the final pellet properties was evaluated. The *in vitro* dissolution behavior was dramatically altered by the drying techniques that were considered. The investigated pellets showed drug release rates that varied as much as 100%. As no polymorphic transitions occurred during drying, we focused on two possible explanations: (a) a change in the drug distribution within the pellets and (b) a change in pellet micro-structure (porosity, pore size). The ibuprofen distribution proved to be homogeneous regardless of the drying conditions. Pellet porosity and pore sizes, however, were modified by the drying process. Our results clearly demonstrate that a single process step, such as drying, can play a crucial role in achieving desired pellet properties and release profiles.

KEY WORDS: desiccation; extrusion/spheronization; fluid bed; lyophilization.

INTRODUCTION

Pharmaceutical pellets are spherical granules that are produced *via* various processes, including wet extrusion/spheronization during which the pellets are first wet-extruded, then spheronized, and, finally, dried. Clearly, the pellet properties are a function of the process parameters and the formulation, *i.e.*, the composition. Typically, studies that investigate the process behavior focus on the extrusion and spheronization steps during which the wet mass is compounded, mixed, kneaded, and shaped. The granulation liquid distribution in the extrudates is assumed to greatly affect the final product's properties (1). However, the granulation liquid needs to be removed in a final step, *i.e.*, drying. Yet only a few studies have focused on the impact of the drying step on the final pellet properties.

Most studies available in the literature investigated pellets that are composed of microcrystalline cellulose and water. Microcrystalline cellulose tends to swell when wetted with water and shrinks again during drying (2,3). A relationship between the drying conditions and the extent of shrinkage was described by several authors (1,4–11). Drying conditions were also shown to affect the final pellet size and the corresponding size distribution (1,4–7,9,11), as well as the pellet micro-structure (3,6–11). Drying-induced differences in the micro-structure significantly influence the pellet's compaction behavior (7–9,12,13) and the active pharmaceutical ingredient (API) release (dissolution) characteristics (7,11,14,15). Additionally, the spatial API distribution, which is expected to vary with the drying conditions (16), may affect the dissolution behavior. For example, Ansari and Stepanek (17,18) prepared pharmaceutical granules *via* wet and melt granulation and tailored the spatial API distribution (*i.e.*, random API dispersion, API located in the shell, API located in the intermediate layer, and API located in the core) by modifying the fluid-bed granulation process or the API particle size. Dissolution times were longer when the API was located in the core and shorter when the API was located in the shell.

When solids (active component, carrier system) are in contact with liquid, certain amounts of the API and the excipients are dissolved. Depending upon the drying conditions (*i.e.*, drying temperature, moisture of drying air, and flow velocity of drying air), the API might be transported with the evaporating liquid. Once the solubility of API exceeds the equilibrium solubility due to liquid evaporation, crystallization occurs. Thereby,

[1] Institute of Pharmaceutical Sciences, Department of Pharmaceutical Technology, University of Graz, Graz, Austria.
[2] Institute for Process and Particle Engineering, Graz University of Technology, Graz, Austria.
[3] Research Center Pharmaceutical Engineering GmbH, Graz, Austria.
[4] Department of Chemical and Biochemical Engineering, Rutgers University, New Brunswick, New Jersey, USA.
[5] To whom correspondence should be addressed (e-mail: eva.roblegg@uni-graz.at)

various spatial API distributions may be obtained as shown for other systems by Lekhal *et al.* (19) and Liu *et al.* (20). In addition to a uniform distribution, egg shell (API is at the surface), egg yolk (API is in the center), and egg white (API is between center and surface) profiles may be obtained, depending on the physical characteristics of the system and the drying conditions. Assuming that API profiles are initially uniform, the final type of API profile is determined during drying by the relative strength of convection, diffusion, and adsorption of API onto the carrier and liquid evaporation rate (19,20). Convection is more pronounced for higher drying rates, when the API is transported toward the outer regions of the carrier, resulting in egg shell profiles. Diffusion dominates at lower drying rates. During the drying process, the drying rate may gradually decrease, and due to the formation of API concentration gradients between the outer and inner carrier regions, an initially formed egg shell profile may become uniform again or egg yolk-like. Additionally, re-crystallization can affect an API profile (20) and/or its dissolution rate.

During pharmaceutical wet granulation, certain amounts of API dissolve in the granulation liquid (depending on the API's solubility), and the dissolved API molecules could be redistributed upon drying (16,21–25). However, to our knowledge, there are no studies that evaluate spatial API distribution in a pellet (prepared by wet extrusion/spheronization) as a function of the drying procedure.

The possible scenarios of how a drying process may influence the pellet's properties are that (1) drying affects the pellet's micro-structure and morphology and/or (2) drying alters the location of the drug inside the pellet. The present study addresses the effect of drying for a specific model system. As a model system, lipophilic matrix pellets consisting of calcium stearate (CaSt) and ibuprofen (26) were prepared *via* a wet extrusion/spheronization process. After spheronization, three drying techniques were applied:

1. Pellets were placed in a desiccator over silica gel at ambient conditions, representing slow drying
2. Fluid-bed drying, representing fast drying
3. Freeze drying (lyophilization) which does not change the structure of the pellets and the initial API distribution

We focused on the influence of drying conditions on the pellet micro-structure (*i.e.*, the pellet pore structure) and on the spatial API distribution. For qualitative API profile determination, *Raman mapping* was used. This technique is frequently applied to elucidate API distribution in tablets (*e.g.*, (27)) and smaller entities, such as supported catalysts (28).

MATERIALS AND METHODS

Materials

Vegetable CaSt (stearic acid 44% and palmitic acid 54%, volume median particle size=16.62 μm, Werba-Chem GmbH, Vienna, Austria) was used as a pellet matrix former. The model drug was ibuprofen (volume median particle size= 104.67 μm, GL Pharma, Lannach, Austria). The powders corresponded to the requirements of the European Pharmacopoeia (Pharm. Eu.). Particle sizes were determined *via* laser diffraction (Helos, Symapetc, GmbH, Clausthal-Zellerfeld, Germany). A mixture of 50 wt.% purified water and 50 wt.% ethanol (Merck, Darmstadt, Germany) was used as a granulation liquid. The dissolution medium was prepared using monopotassium phosphate and sodium hydroxide (both Merck, Darmstadt, Germany). For the HPLC analysis MQ water, triethylamine, orthophosphoric acid 85%, and acetonitrile (all Merck, Darmstadt, Germany) were used as the mobile phase.

Primary Particle Characterization

Solubility Measurements

In order to determine the solubility of ibuprofen in the granulation liquid and in the dissolution medium, saturated solutions were prepared and stirred for 48 h at room temperature. Samples of 1 ml were withdrawn at certain time points; filtered; diluted, if necessary; and quantified *via* UV/VIS spectrometry at 221 nm.

Contact Angle Measurements

Contact angles of calcium stearate, ibuprofen, and the CaSt/ibuprofen mixture used for extrusion with water, ethanol, and 50% ethanol were investigated. The contact angles of powder compacts were evaluated with the *EasyDrop* System (Krüss, Hamburg, Germany) equipped with a CCD camera. Values of the contact angles were obtained *via* data fitting using the *circle fitting* tool. All experiments were repeated six times.

Swelling Measurements

The swelling properties of CaSt in water, ethanol, and in 50% ethanol were investigated. Certain amounts of CaSt were placed in a graduated cylinder and liquid was added. The cylinder was sealed and gently shaken to prepare a suspension. The suspension was left for 24 h to let the particles swell and settle. The apparent volume of the settled particles was metered, and the swelling ratio Q_d was calculated:

$$Q_d = \frac{|V_1 - V_2|}{V_1} \tag{1}$$

where V_1 and V_2 are the volumes of the initially dry and the swollen (after 24 h) powder, respectively.

Differential Scanning Calorimetry

To elucidate any possible interactions between ibuprofen and CaSt that might occur at elevated temperatures (*i.e.*, during fluid-bed drying), differential scanning calorimetry (DSC) measurements were performed. Samples were placed into aluminum pans covered with aluminum caps. The pans were positioned in a DSC 204 F1 Phoenix (Netzsch, Selb, Germany) and heated to 40°C at 1 K/min. Subsequently, samples were kept at constant temperature for 20 min. All measurements were performed in triplicate under nitrogen atmosphere (nitrogen flux of 20 ml/min).

Pellet Preparation and Characterization

Pellet Preparation

The formulation and process parameters were adapted from our previous work (26). CaSt and ibuprofen were initially dry blended in a cube mixer (UAM Pharmag, Pharmatest, Hainburg, Germany) at 300 rpm for 20 min. One hundred grams of the powder mixture was wetted in an open planetary mixer (Kenwood Chef, Kenwood, Hampshire, UK) with 35 g of the granulation liquid (*i.e.*, 50% ethanol). The wet mass was transferred into a single-screw extruder (Extruder Pharmex T35, Gabler Maschinenbau GmbH, Lübeck, Germany) equipped with a 1.5-mm multi-hole die plate (1.5 mm diameter, 2 mm in length, 400 holes). Extrusion was performed at a constant screw speed of 30 rpm. The extrudates were instantly placed into a spheronizer containing a cross-hatched friction plate, where they were rounded at 300 rpm for 16 min. The process parameters are summarized in Table I. A moisture halogen analyzer (HR 73 Halogen Moisture Analyzer, Mettler Toledo International, Inc., Columbus, OH, USA) was used to determine the moisture content of the wet mass, the extrudates, and the pellets after spheronization.

Drying Processes

After spheronization, three drying techniques were used to remove the granulation liquid: desiccation (D), fluid-bed drying (FB), and lyophilization (L). For each drying method, two batches were prepared. The process parameters are summarized in Table I.

Drying via Desiccation over Silica Gel

After spheronization, the pellets were transferred into a flat bottom bowl and placed in a desiccator over silica gel orange at ambient temperature and pressure. The diameter of the pellet bed was 17 cm, and the height was approximately 0.5 cm. To determine the moisture drop as a function of drying time, one additional batch was prepared. At certain time intervals, samples were taken from the center of the pellet bed using a spatula. The moisture content was determined, and drying was continued until a liquid content below 1.5% was reached.

Fluid-Bed Drying

For the fast drying process, the pellets were transferred into a fluid-bed apparatus (Mycrolab, Oystar Hüttlin, Schopfheim, Germany). After preheating (inlet air temperature=40°C, time=20 min), the pellets were dried at the inlet air temperature of 40°C for 20 min to reach the moisture content below 1.5%. The inlet air flow was 45 m^3/h during the entire process.

Lyophilization

The pellets were placed into kidney-shaped bowls with a flat bottom and immersed into liquid nitrogen (−196°C) for 15 min. The frozen pellets were transferred into a freeze drier (LYOVAC GT 2, Steris, Köln, Germany). Vacuum was applied (pressure below 10 mbar), and finally, the pellets were dried for 48 h at ambient temperature to reach the moisture content below 1.5%.

Pellet Shrinkage Behavior

The shrinkage behavior during liquid removal was investigated for the pellets dried *via* desiccation and fluid-bed drying. The pellets were prepared as described above. After spheronization, the volume of 50 g of the wet pellets was determined. Once the pellets were dried (see above), the volume was measured again. The volume reduction was calculated according to Eq. (1), where V_1 is the volume of the dry pellets and V_2 is the volume of the wet pellets. All experiments were performed in triplicate.

Pellet Size and Shape

In order to determine the pellet size distribution, sieve analysis was carried out according to Pharm. Eu. 6.0 2.9.38 using analytical DIN sieves with a $\sqrt{2}$ progression (sieve openings 0.5–2.0 mm). The fraction between 1.4 and 1.8 mm was denoted as the yield fraction, which was divided using a rotary cone divider to obtain representative samples for further characterization studies.

The shape and size were investigated for at least 500 pellets using the dynamic image processing system QicPic (Symapetc, GmbH, Clausthal-Zellerfeld, Germany) equipped with a dry dispersing unit Rhodos/L. The pellets were dispersed with the pressure of 0.2 bar, and their

Table I. Process Parameters Used for the Preparation of the Lipophilic CaSt Pellets

	Wetting	Extrusion		Spheronization		Drying		
Formulation	Amount of granulation liquid (g/100 g)	Die hole size (mm)	Screw speed (rpm)	Speed (rpm)	Time (min)	Method	Temperature (°C)	Time (h)
D1	35	1.5	30	300	16	Desiccation	Ambient	168
D2	35	1.5	30	300	16	Desiccation	Ambient	168
FB1	35	1.5	30	300	16	Fluid-bed drying	40[a]	0.67
FB2	35	1.5	30	300	16	Fluid-bed drying	40[a]	0.67
L1	35	1.5	30	300	16	Lyophilization	−196[b]	48
L2	35	1.5	30	300	16	Lyophilization	−196[b]	48

[a] The temperature refers to the inlet air temperature
[b] The pellets were frozen with liquid nitrogen

images were automatically analyzed. Thereby, the size (Ferret's diameter) and shape (aspect ratio, AR) distributions were obtained. Each batch was analyzed three times.

Small- and Wide-Angle X-ray Scattering Measurements

In order to determine if the API altered its crystal state during preparation, small- and wide-angle X-ray scattering measurements (SWAXS) were performed. A high-flux laboratory small- and wide-angle X-ray scattering camera S3-Micro (Hecus X-Ray Systems, Graz, Austria) equipped with a high-brilliance micro-beam delivery system was used. The samples were filled into glass capillaries (inner diameter 2 mm), sealed with wax, and placed into the SpinCap (*i.e.*, a rotating capillary). The wavelength λ was 1.54 Å, and the SAXS curves were recorded with a 1D-detector (PSD-50, Hecus X-ray Systems, Graz, Austria) in the angular range between 0.06° and 8°. The exposure time was 500 s, and the beam size was 200 μm. All measurements were performed in triplicate at room temperature.

Raman Mapping

Raman mapping was used to measure the API distribution in the dry pellets. The pellets were cut microtomically (Felmi, Graz, Austria), and Raman spectra were recorded using a Jobin Yvon Labram HR (Horiba Co., Ltd., Kyoto, Japan) equipped with a 633-nm helium–neon laser in combination with an Olympus BX41 microscope. Regions of 100×100 μm along the pellet diameter of the pellet cross section (Fig. 1) were scanned. Mapping was performed using Swift® routine with 0.7 s integration time per point. Spectra were recorded in a region ranging between 100 and 2,300 cm^{-1} with a resolution of 2.5 cm^{-1}. The ibuprofen distribution was evaluated by comparing the mean spectra of each region with the spectra of the raw materials.

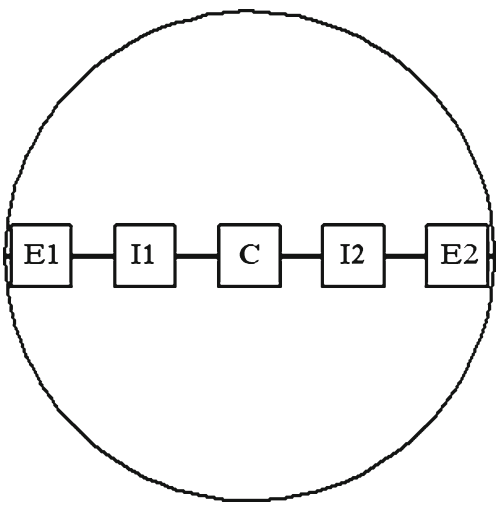

Fig. 1. Schematic illustration of the pellet cross section used for Raman mapping. Regions of 100×100 μm were scanned: *E* edge; *I* intermediate, and *C* center. The mean spectra of each region were calculated

Pellet Density and Porosity

The true pellet density (ρ_{ture}) was determined using a helium pycnometer (AccuPyc II 1340, Micromeritics, Norcross, GA, USA). The pycnometer used 20 purges at 19.5 psi and five analytical runs at 19.5 psi with an equilibration rate of 0.0050 psi/min. The pellet volume was measured and the pellet density was calculated. Each experiment was performed in triplicate. Additionally, the densities of the primary particles (*i.e.*, CaSt and ibuprofen) were determined for comparison reasons.

The volume of the open pores (V_{pore}) was determined with a mercury porosimeter (Quantachrome Poremaster 60-GT; Quantachrome GmbH & Co. KG, Odelzhausen, Germany). The pellets were transferred into a sample chamber, which was subsequently evacuated and filled with mercury according to the manufacturer's instructions. Experiments were conducted at 20°C. The porosity (ε) was calculated by combining helium pycnometry and mercury porosimetry as follows:

$$\varepsilon = \frac{V_{pore}}{V_{pore} + \frac{1}{\rho_{true}}} \times 100\% \quad (2)$$

It should be noted that this calculation assumes the absence of any closed pores.

Scanning Electron Microscopy

After sputter coating with chromium, the pellets were examined in a scanning electron microscope (SEM; Zeiss Ultra 55, Carl Zeiss NTS GmbH, Oberkochen, Germany).

Crushing Strength

The crushing strength was determined using a rheometer (MCR 301, Anton Paar, Graz, Austria) equipped with a parallel plate measuring system (PP25) in the non-rotational mode. For each batch, 70 pellets were randomly taken. The pellets were manually placed in the center of the lower plate. The upper plate was moved down at a constant velocity of 0.5 μm/s until the gap distance of 1.2 mm was reached, at which fracture was certain to occur in every pellet.

The values for crushing strengths (σ) were calculated from the force displacement plots by using the following equation (29):

$$\sigma = \frac{1.6F}{\pi d^2} \quad (3)$$

where F is the maximal force of plastic deformation upon fracture and d is the gap distance at the beginning of the deformation, *i.e.*, equal to the particle diameter if perfectly round.

In Vitro Drug Release Characteristics

Dissolution testing was performed using the United States Pharmacopoeia (USP) apparatus I (Pharma Test Type PTWS III C, Pharma Test Apparatebau AG, Hainburg, Germany). Following the USP XXVIII monograph for ibuprofen tablets, 900 ml of pH 7.2 monopotassium phosphate buffer

was applied as a dissolution medium. In order to ensure sink conditions, 500 mg pellets were used. The temperature was 37±0.5°C and the stirring speed was 100 rpm. Samples of 1 ml were withdrawn from the dissolution media at certain time intervals and analyzed *via* reversed-phase high-performance liquid chromatography (RP-HPCL). Each batch was tested six times.

RP-HPLC Analysis

Ibuprofen concentrations were determined by adapting an HPLC method developed by Ravisankar *et al.* (30). A Merck system (Merck Hitachi, Merck Serono Co., Ltd., Tokyo, Japan) was used at 25°C. The mobile phase consisted of 0.2% triethyl amine and acetonitrile (1/1 *v*/*v*). The pH was adjusted to 3.4 with orthophosphoric acid 85%. The injection volume was 20 μl, and the flow rate was 1.2 ml/min. Ibuprofen was detected with a UV/VIS detector at 215 nm. As an external standard, a calibration curve ranging from 2 to 10 μg/ml ibuprofen was generated.

The limit of detection and the limit of quantification (LOQ) were determined according to a guideline of the International Conference on Harmonization (31). Values below LOQ were set to zero.

Investigation of the Drug Release Mechanism

The drug release mechanism was investigated *via* fitting to existing models (Eqs. 4–6) using Sigmaplot Version 11 (Systac Software Inc, Chicago, USA). The following release kinetics was considered:

Zero-order release

$$A_t = k_0 t, \tag{4}$$

where A_t is the fractional cumulative amount of API dissolved at time t, k_0 is the zero-order release constant, and t is the time.

Higuchi model

$$A_t = K_H \sqrt{t}, \tag{5}$$

where K_H is the Higuchi dissolution constant.

Korsmeyer–Peppas model

$$A_t = K t^n, \tag{6}$$

where K is a constant incorporating structural and geometric characteristics and n is the release exponent.

RESULTS

Primary Particle Characterization

Pure water did not wet ibuprofen and calcium stearate (contact angles above 90°; Table II). However, all contact angles of ethanol and 50% ethanol were well below 90°. Additionally, ibuprofen shows a high solubility in 50% ethanol (*i.e.*, 48.06±1.796 g/l) and calcium stearate swells in pure ethanol (Q_d=3.96±0.44). The swelling capacity of CaSt in deionized water or in 50% ethanol could not be determined. It was impossible to prepare a suspension for water, since CaSt remained on the water surface. For 50% ethanol, the powder particles failed to settle within 24 h, and thus, it was impossible to determine the volume of the swollen compound despite the obvious swelling.

DSC measurements were performed to detect any interactions that might occur during fluid-bed drying. Figure 2 shows the DSC signal. It does not reveal any peaks or glass transitions, indicating that neither polymorphic transitions nor interactions between ibuprofen and calcium stearate occurred under the investigated conditions.

Pellet Preparation and Characterization

Pellet Preparation

The pellets were prepared *via* the extrusion/spheronization process. During extrusion, the wet mass was compacted and shaped into extrudates that were relatively short and exhibited some shark skinning (Fig. 3). The comparison of the values of the moisture contents (for the wet mass, the extrudates, and the wet pellets) of two corresponding batches showed small differences (Table III). This might be due to slight inhomogeneities in the granulation fluid distribution. As can be seen, the moisture content dropped throughout the preparation process, and during spheronization, a significant amount of the granulation liquid evaporated (*i.e.*, around 55%).

Drying Processes

In all cases, the drying process continued until the moisture content was below 1.5% (Table III). The comparison between the different drying techniques indicated that the final moisture content was slightly higher for the pellets dried in the desiccator (*i.e.*, 0.72 and 1.08% for D1 and D2) than for those dried in the fluid bed (*i.e.*, 0.58 and 0.51% for FB1 and FB2) and in the freeze drier (*i.e.*, 0.21 and 0.4% for L1 and L2).

The drying profile of the pellets dried *via* desiccation showed that after 7 days, the moisture content was below 1.5% (Fig. 4a). The moisture content dropped rapidly within the first 24 h (*i.e.*, from 9.5 to 2.7%) and then slowly decreased to zero. In order to investigate whether a constant rate period was present, the rate of change in the pellets' moisture content was calculated and plotted against time (Fig. 4b). It shows that no constant rate period existed. The shrinkage experiments demonstrated that the pellet volume considerably decreased during liquid removal in the desiccator (*i.e.*, shrinkage of 13.8 ±1.30%).

The drying process in the fluid-bed system was significantly faster (*i.e.*, 40 min to reach the moisture content below 1.5%). After the preheating period (*i.e.*, first 20 min), the product temperature was 38.5 and 38.4°C for FB1 and FB2, respectively. Pellet shrinkage was lower in comparison to drying *via* desiccation (*i.e.*, 8.36±0.442%).

Lyophilization was faster than desiccation but slower than fluid-bed drying: After 48 h, the pellets had the moisture content below 1.5%. During freeze drying, no liquid was involved resulting in minimal capillary flow. Hence, minimal pellet shrinkage occurred.

Table II. Contact Angles and Standard Deviation of the Primary Powders with Water, Ethanol, and 50% Ethanol

Powder substance	Contact angle with water (deg) (SD)	Contact angle with ethanol (deg) (SD)	Contact angle with 50% ethanol (deg) (SD)
Ibuprofen	91.6 (3.3)	Well below 90[a]	25.6 (2.4)
Calcium stearate	113.5 (3.8)	34.1 (0.95)	60.8 (2.5)
Mixture ibuprofen/calcium stearate	111.2 (4.4)	31.1 (0.83)	57.2 (1.9)

[a] Analysis of the video was impossible due to a very fast drop penetration

Pellet Size and Shape

The pellet size distribution of the whole batch was determined *via* sieve analysis. The yield fraction, which was used for subsequent characterization studies, was denoted as the fraction between 1.4 and 1.8 mm. For the pellets dried *via* desiccation, 68% (D1) and 72% (D2) were in this yield fraction. FB1 and FB2 showed similar results (*i.e.*, 65 and 67%). The findings of the sieve analyses demonstrated that both drying techniques also produced pellets with diameters below 1.4 mm and above 1.8 mm. However, more pellets larger than 1.8 mm were prepared *via* fluid-bed drying (10 and 9%), compared to desiccation (3 and 4%). The pellets dried *via* lyophilization showed somewhat lower yields—62 and 64% for L1 and L2, respectively. More pellets with a diameter of over 1.8 mm were formed (*i.e.*, 16 and 15%).

The Feret's diameter and the aspect ratio were only determined for pellets in the desired yield fraction. The results for the median maximal Feret's diameter and the median AR are summarized in Table IV. The median Feret's diameter was similar for all batches, which was expected since only the yield fraction was evaluated. The aspect ratio was well below 1.2 for all pellets under investigation.

SWAXS Measurements

In order to determine the structure (crystal or amorphous) of solid ibuprofen after drying, SWAXS was used. Since the formulation was composed of two crystalline primary powders (*i.e.*, ibuprofen and calcium stearate), some Bragg peaks (32) may have overlapped, especially in the molecular WAXS angular range. Consequently, the analysis was confirmed by applying the SAXS angular range, which depicts all larger crystals and their internal order (33). The API showed a clear "fingerprint" peak in the SAXS region at 14.6 Å, which did not overlap with any corresponding peak of CaSt. The decreased intensity of the peak at 14.6 Å (Fig. 5) of the pellet samples compared to the pure API was attributed to the fact that the pellets contained only 20% of ibuprofen. Nevertheless, the Bragg peak characteristic for ibuprofen was clearly identified. Therefore, it was concluded that none of the drying processes significantly or detectibly changed the drug's crystal form.

Raman Mapping

Ibuprofen showed a characteristic band between 1,170 and 1,225 cm^{-1} and CaSt between 1,270 and 1,310 cm^{-1}. Here, no overlapping with the spectra of the other compound or the epoxy resin, into which the pellets were embedded, was found. The API distribution was calculated based on the intensities of those peaks.

Figure 6 displays the mean spectra of the regions along the pellet cross section (see Fig. 1). For all drying methods, the spectra of one batch (*i.e.*, D2, FB2, and L1) are shown, since no differences were found between the batches. No significant spatial accumulation of ibuprofen was found, which indicated close-to-uniform API profiles for all drying methods. However, amplifications of the ibuprofen peak (Fig. 6, right-hand side) did show—at least in the case of fluid-bed drying—differences in the concentration, which may be in part due to drying or rather other effects (such as pores resulting in a non-planar focal plane) than to regions of higher ibuprofen concentrations. The results of the Raman mapping imply that the ibuprofen distribution in the CaSt pellets was not significantly affected by the drying technique.

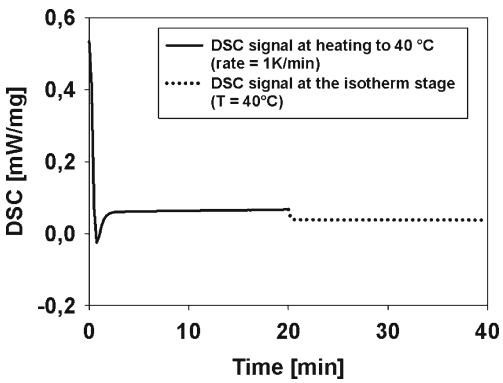

Fig. 2. DSC thermogram of the ibuprofen/CaSt mixture, simulating the conditions during fluid-bed drying. The DSC signal is a straight line that shows no interactions under the applied conditions

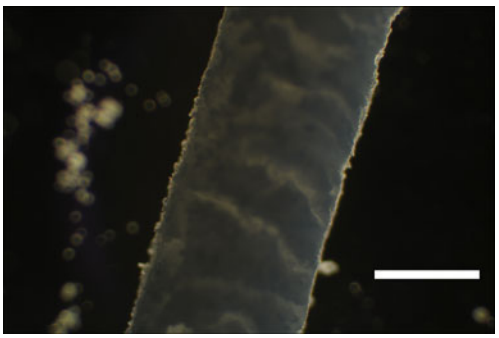

Fig. 3. Microscope image of a wet extrudates obtained after 30 s of extrusion. The extrudates showed some extent of shark skinning. *Bar scale* 1 mm

Table III. Moisture Contents of the Products at Each Preparation Step

Formulation	Moisture content of wet mass (%)	Moisture content of extrudates (%)	Moisture content of wet pellets (%)	Moisture content of dry pellets (%)
D1	21.9	19.3	8.3	0.72
D2	22.7	19.6	9.1	1.08
FB1	23.4	20.3	8.3	0.58
FB2	22.9	20.5	9.7	0.51
L1	22.7	20.9	9.4	0.21
L2	23.0	19.6	8.5	0.40

Pellet Density and Porosity

The densities of the pellets were determined *via* helium pycnometry (Table IV). Additionally, the density of the powder mixture used for extrusion was determined, *i.e.*, 1.0645± 0.0006 g/cm^3. The densities of D1 and D2, and L1 and L2 were similar to the density of the powder mixture. The densities of the fluid-bed-dried pellets, however, were lower.

The pore size distributions, obtained *via* mercury porosimetry, revealed that all pore diameters ranged between 20 nm and 5 μm. The median pore diameters were estimated, and it was established that the pellets dried *via* desiccation and lyophilization exhibited similar pore diameters (Table IV). The pore diameter was greater for the pellets dried in the fluid-bed apparatus. Pellet porosity (Table IV) was the highest for the pellets dried *via* lyophilization. The pellets dried *via* desiccation and fluid-bed drying showed similar porosity values, although the shrinkage experiments demonstrated that volume reduction during drying was lower for the fluid-bed process (*i.e.*, 13.8% for desiccation and 8.36% for fluid-bed drying).

Scanning Electron Microscopy

All pellets were spherical in shape (Fig. 7 A1), and the surface of pellets dried *via* desiccation or lyophilization (Fig. 7 A1) was rather smooth. Pellets that were dried in the fluid-bed apparatus revealed kind of a pattern on their surface that was not detected for pellets dried *via* desiccation and lyophilization (Fig. 7 A1). All batches exhibited a distinct pore system on their surface (Fig. 7 A2) and inside (Fig. 7 B1, B2). Amplifications of the surface (Fig. 7 A2) and the pellet cross section (Fig. 7 B2) showed that the drying procedure qualitatively influenced the pellet morphology. Apparently, the pore size was smaller for L1 and L2, and pores were distributed more homogeneously in comparison to D1, D2, FB1, and FB2. However, it should be noted that the SEM images only qualitatively describe the micro-structure of a single pellet.

Crushing Strength

The pellet crushing strength decreased in the order D, FB, and L (Table IV). All force displacement diagrams revealed elastic–plastic deformation followed by the initial breakage of the pellet (data not shown). As the upper plate was moved further down, additional breakage points were observed.

In Vitro Drug Release Characteristics and Investigation of the Drug Release Mechanism

The equilibrium solubility of ibuprofen in the dissolution medium was 3.69±0.12 g/l and more than 30-fold higher than the ibuprofen concentration at 100% dissolution (*i.e.*, 0.11 g/l). Thus, perfect sink conditions were maintained during the entire experiment.

All drug release profiles showed prolonged drug release (Fig. 8). However, the pellets showed significantly different release rates depending on the drying method. Within 6 h, slightly more than 10% of the API was released from the pellets dried *via* desiccation. The pellets dried in the fluid-bed apparatus and in the freeze drier showed higher release rates. After 6 h, around 20 and 27% of ibuprofen were found in the dissolution media for FB and L, respectively. *t* tests were performed to identify statistically significant differences ($p<0.05$) in the amount of ibuprofen released between the two batches dried using the same method. For D, no statistically significant

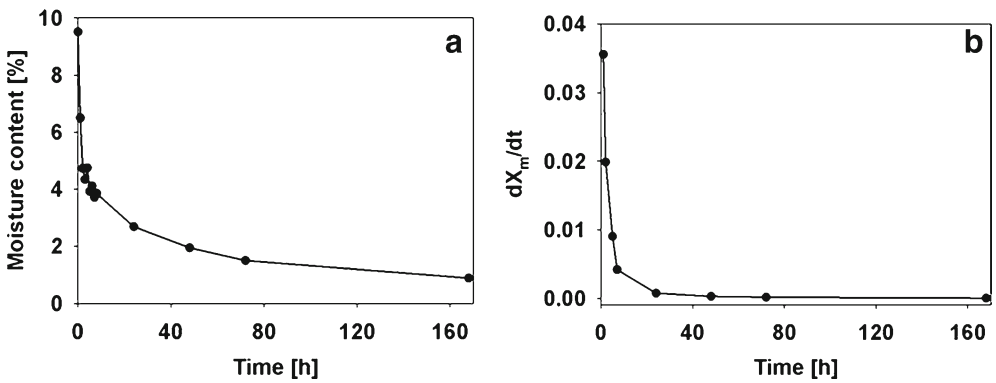

Fig. 4. Drying profile over 7 days for pellets dried *via* desiccation: **a** loss of moisture content as a function of time, **b** change of moisture content (X_m) over time

Table IV. Results of the Pellet Characterization Studies

Abbreviation	$d_{Fer,50}$ (μm) (SD)	AR_{50} (−)	ρ_{true} (g/cm^3) (SD)	$d_{pore,50}$ (μm)	ε (%)	σ (MPa) (SD)
D1	1,656.8 (11.45)	1.112	1.0578 (0.0065)	0.25	18.6	0.420 (0.100)
D2	1,635.7 (3.010)	1.100	1.0693 (0.0022)	0.24	18.2	0.392 (0.0843)
FB1	1,672.3 (12.22)	1.068	1.0016 (0.0147)	0.33	19.3	0.315 (0.0538)
FB2	1,644.5 (8.300)	1.095	1.0342 (0.0113)	0.48	18.6	0.212 (0.0364)
L1	1,664.0 (8.280)	1.069	1.0658 (0.0015)	0.20	23.9	0.148 (0.0710)
L2	1,677.8 (12.32)	1.089	1.0653 (0.0007)	0.18	25.2	0.154 (0.0803)

$d_{Fer,50}$ median Feret's diameter, AR_{50} median aspect ratio, ρ_{true} "apparent" true density, $d_{pore,50}$ median pore diameter, ε porosity, σ crushing strength

differences were found at any time point. For FB and L, however, statistically significant differences were detected at lower time points (*i.e.*, below 20 min). This may be attributed to low initial API concentrations, at which small deviations are significant. The Korsmeyer–Peppas model described the release mechanism best for all batches (R^2>0.99; Table V).

DISCUSSION

Lipophilic calcium stearate/ibuprofen pellets were prepared *via* a wet extrusion/spheronization process. During the wetting step, the primary powders (*i.e.*, calcium stearate and ibuprofen) and the granulation liquid (*i.e.*, 50% ethanol) were combined. It was expected that during the wetting step, the powder mass was wetted by the alcoholic portion of the granulation fluid, since the values of the wetting angles were below 90° (Table II). During wetting, ibuprofen was likely to be dissolved in the granulation fluid due to its high solubility in 50% ethanol (*i.e.*, 48.06±1.796 g/l). Assuming that the temperature of the granulation liquid was 20°C (corresponding to the density of 0.914), it can be estimated that about 9% of the granulated ibuprofen was dissolved. Furthermore, calcium stearate swelled in 50% ethanol and was likely to shrink again during granulation liquid removal.

During extrusion, the wet mass was compacted and shaped into extrudates that were relatively short, which may be due to the low length-to-diameter (*L*/*D*) ratio of the die holes of the screen (*i.e.*, 1.3) (34). Typically, wet masses are more densified in dies of greater lengths resulting in longer extrudates. Shark skinning, which might be due to the low *L*/*D* ratio (34), was observed (Fig. 3). Since the extrusion speed was comparatively low, excessive shark skinning did not occur, which was in agreement with previous findings (34).

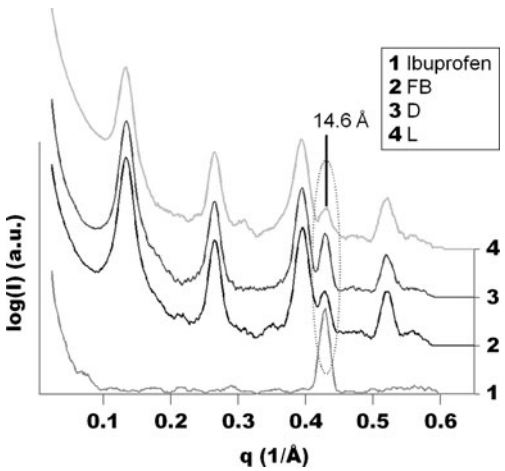

Fig. 5. SAXS spectra of the pure API (ibuprofen) and the pellets dried *via* different techniques. *FB* fluid bed, *D* desiccation, *L* lyophilization

After spheronization, three drying techniques (*i.e.*, desiccation, fluid-bed drying, and lyophilization) were applied to remove the granulation liquid. During drying, dissolved ibuprofen might be redistributed and/or calcium stearate might shrink. Dissolved ibuprofen molecules may be transported toward the pellet surface with the evaporating liquid. As soon as a saturated solution is generated, ibuprofen may re-crystallize close to the pellet surface. Thereby, egg shell-like ibuprofen profiles may potentially form. However, since only 9% of ibuprofen dissolved, differences in the API distributions were minor. This issue will be addressed in further studies using pellets with lower drug loadings.

Figure 4a shows the drying profile of the pellets dried *via* desiccation at ambient conditions. Generally, drying profiles consist of three stages: the preheating stage, the constant rate stage, and the falling rate stage. During the first stage, the pellets are heated with a drying medium and, as the temperature rises, the drying rate increases. Since desiccation was performed at ambient conditions, no preheating stage was observed. During the second stage, vapor is removed from the saturated surface. The liquid transport inside a pellet is sufficient to keep the surface saturated, and moisture is removed *via* a capillary flow. When the liquid transport inside the pellet is no longer sufficient, the drying rate decreases, and the falling rate stage begins at this critical moisture content. However, for the desiccation process, no constant rate stage was detected (Fig. 4b). Due to the low initial moisture content (*i.e.*, moisture content after spheronization—8.3 and 9.1% for D1 and D2; Table III), the pellet surface may have not been saturated. Another reason for the absence of the constant rate period might be contraction of the pellets during drying (3). Thereby, the pellet surface area was gradually altered and a non-linear shape of the drying profile was observed. Indeed, the shrinkage experiments demonstrated that the pellet volume was considerably decreased during liquid removal in the desiccator (*i.e.*, shrinkage of 13.8±1.30%). Due to markedly higher drying rates during fluid-bed drying compared to desiccation, shrinkage was less pronounced (*i.e.*, shrinkage by 8.36±0.442%) (9) than for the pellets dried in the desiccator. During lyophilization, the granulation liquid is removed *via* sublimation, which results in minimal pellet contraction (6,9).

In order to ensure that no chemical and physical interactions between ibuprofen and calcium stearate occurred during the fluid-bed process (inlet air temperature 40°C), DSC measurements were performed. APIs and excipients may

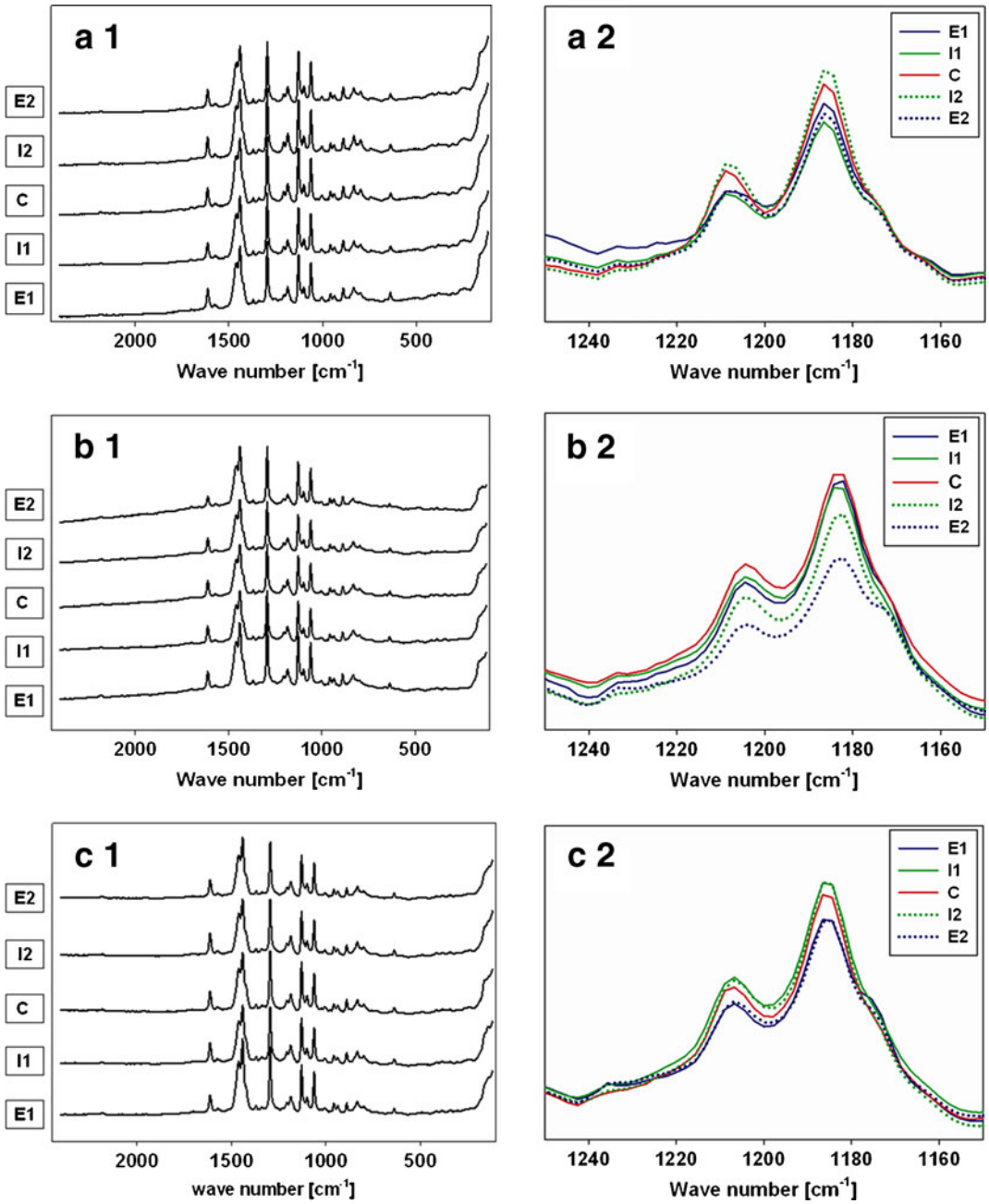

Fig. 6. Mean spectra of the regions along the pellet cross section, which were investigated *via* Raman mapping: *a* desiccation; *b* fluid bed; *c* lyophilization; *1* entire spectrum; *2* amplification of the characteristic ibuprofen peak ranging between 1,170 and 1,225 cm^{-1}: Ibuprofen was homogeneously distributed in the pellets (uniform ibuprofen profile)

undergo a polymorphic transition during drying at elevated temperatures (see, for example, (35–39)). Thereby, the final pellet properties, such as the drug release behavior, may be changed (38). Since the DSC graphs in Fig. 2 do not show any peaks, it can be concluded that neither polymorphic transitions nor interactions between ibuprofen and calcium stearate occurred during fluid-bed drying. It was assumed that fluid-bed drying did not influence (a) the crystalline, (b) the chemical, and (c) the physical state of the used powders.

The Raman spectra (Fig. 6 A1, A2) indicated uniform ibuprofen profiles after desiccation. As stated above, in the course of desiccation, the constant rate period was missing (Fig. 4b), during which dissolved components are typically transported toward the outer regions by convection. Thus, convective effects were low, which resulted in the reduced transport of ibuprofen toward the pellet surface and, consequently, in the uniform ibuprofen profiles (19,20), assuming ibuprofen was homogenously distributed throughout the wet pellets.

Due to the increased evaporation rate during fluid-bed drying, the convective flow transporting ibuprofen toward the pellet surface was greatly enhanced, which could lead to egg shell-like profiles. However, it is known that ibuprofen causes phase separation of a 50% ethanol solution (*i.e.*, the granulation liquid) between 25 and 40°C (40). Jbilou *et al.* (41) demonstrated that ibuprofen crystallized in the aqueous phase (due to its poor water solubility) when phase separation

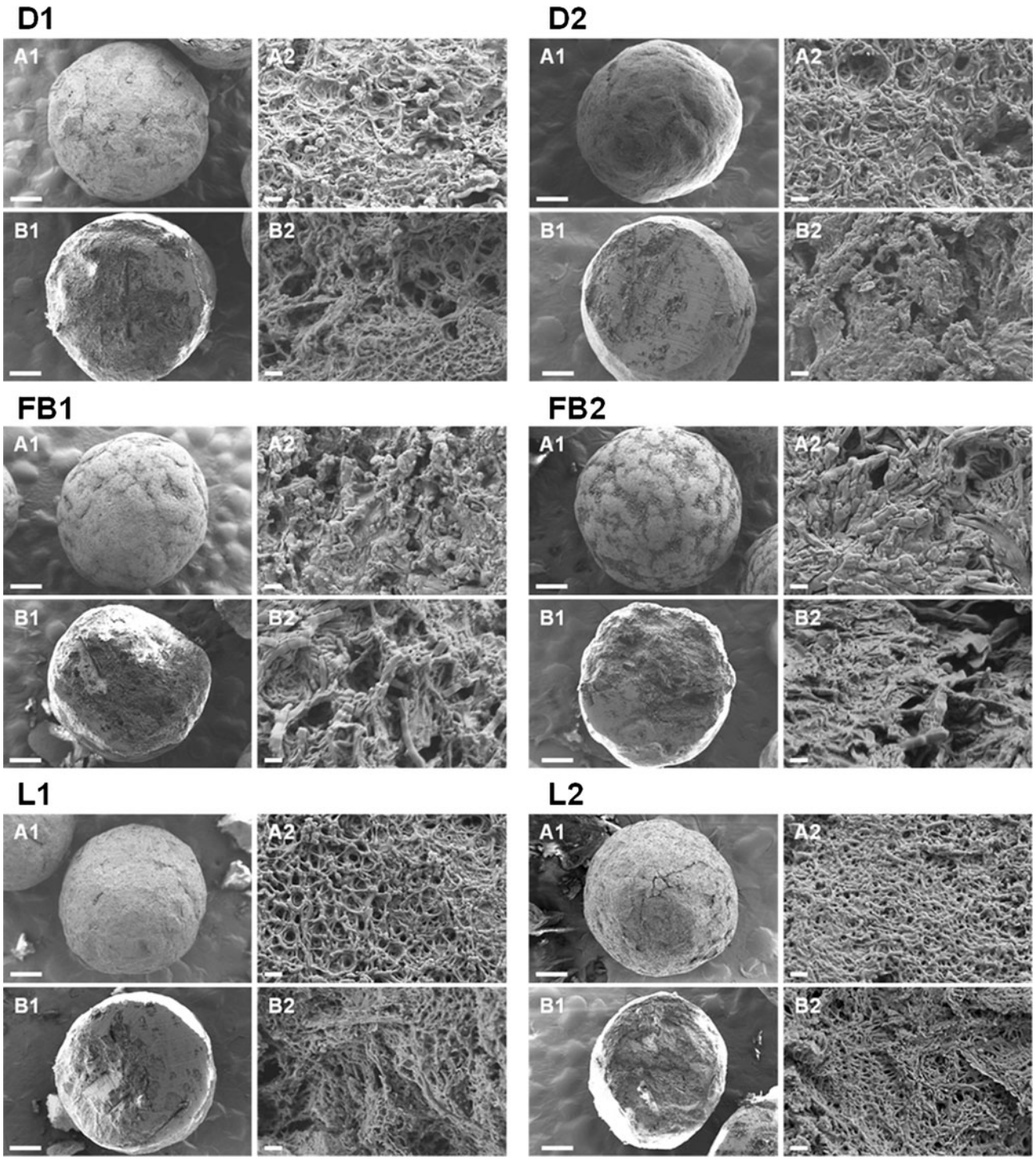

Fig. 7. Scanning electron microscopy images: *A* pellet surface; *B* pellet cross section; *1* entire pellet, *bar* size 300 μm; *2* amplification, *bar* size 1 μm

occurred. Hence, it may be assumed that ibuprofen crystallized in the aqueous phase and was therefore not transported toward the external pellet surface. Thus, close-to-uniform profiles were obtained (Fig. 6 B1, B2). During lyophilization, redistribution of ibuprofen was suppressed due to the absence of any liquid, and the final ibuprofen profile was uniform again (Fig. 6 C1, C2).

These findings demonstrate that the drying conditions under consideration affected the extent of the pellet shrinkage but not the final ibuprofen profile. Typically, pellet shrinkage is likely to influence the pellet size and corresponding size distribution and/or the pellet micro-structure (*i.e.*, pellet porosity). The particle size distributions were in accordance with the shrinkage experiments. Since the pellets shrunk to the greatest extent during desiccation (*i.e.*, by 13.8±1.30%), the lowest amount of pellets with a diameter above 1.8 mm (*i.e.*, upper limit of yield fraction) was obtained (*i.e.*, 3 and 4%). In contrast, during lyophilization, the extent of shrinkage was minimal, and thus the highest amount of pellets larger than 1.8 mm was produced (*i.e.*, 16 and 15%). However, the drying technique

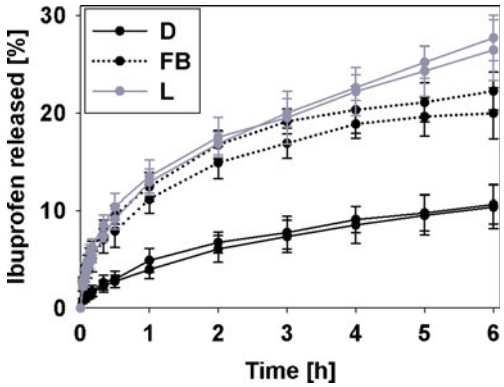

Fig. 8. *In vitro* dissolution profiles of the pellets dried *via* desiccation (*D*), fluid-bed drying (*FB*), and lyophilization (*L*). For each drying technique, two dissolution profiles are shown. $n=6$

had no significant impact on the pellet shape (represented by the aspect ratio). The aspect ratio was well below 1.2 for all batches (Table IV).

As pellets contract during drying, the pellet porosity might be altered. Typically, pellet porosity is inversely proportional to pellet shrinkage. Consequently, the pellet porosity was the highest after lyophilization (*i.e.*, 23.9 and 25.2% for L1 and L2) and the lowest after desiccation (*i.e.*, 18.6 and 18.2% for D1 and D2). Surprisingly, FB1 and FB2 exhibited porosities similar to D1 and D2 (*i.e.*, 19.3 and 18.6%), although the shrinkage was less pronounced during fluid-bed drying (*i.e.*, 8.36±0.442% for fluid-bed drying *versus* 13.8±1.30% for desiccation). This deviation arises from the limitations of the analytical methods used to determine the pellet porosity (*i.e.*, helium pycnometry and mercury porosimetry). Both helium pycnometry and mercury porosimetry can only capture open pores. To identify a closed pore formation, the density of the physical powder mixture (*i.e.*, 1.0645±0.0006 g/cm^3) was determined. It was higher than the density of the fluid-bed-dried pellets, which implies the formation of closed pores. During fluid-bed drying, the pellets randomly collided inducing a certain amount of compaction. Thereby, the pores were likely to be closed, and air pockets (closed pores) were created. The closed pores of the fluid-bed-dried pellets did not contribute to the porosity, and thus, the porosities of fluid-bed-dried pellets were higher than those determined *via* mercury porosimetry and helium pycnometry, explaining the too low measured porosity. Differences in the pellet porosity affect the pellet crushing strength. The strength of individual pellets differs due to the variations in micro-structure attributed to (a) distribution and orientation of bonds, (b) defects, (c) strength of the original crystals, and (d) the pore size distribution. Randomly distributed inhomogeneities may also have an impact on the pellet breakage behavior. The low crushing strength of the pellets dried *via* lyophilization can be attributed to comparatively high porosities. Pores can be regarded as crack release zones, where the highest local stress is generated and fracture initiates from this zone. Since the contact points of the primary particles are decreased at higher porosities (42), lower forces are required upon pellet breakage. The decreased crushing strength of the pellets dried in the fluid bed compared to desiccation might be due to mechanical effects during drying, which caused the formation of cracks or other changes in the pellet micro-structure. The crushing strength varied for the two batches dried in the fluid bed, which might indicate that there was a difference in the process of the closed-pore formation. Moreover, the strength of granules is a function of the granule moisture content (*e.g.* (43)). In the present study, the pellet crushing strength increased (Table IV) as the pellet moisture content increased (Table III).

The *in vitro* dissolution profiles (Fig. 8) show that the drying conditions had a dramatic impact that may be due to (a) polymorphic transitions of ibuprofen during pellet preparation (38), (b) differences in the ibuprofen profile (18), and/or (c) differences in the pellet micro-structure (7,11,14,15). *Via* SWAXS analysis, it was confirmed that no polymorphic transition occurred during any of the preparation processes. The ibuprofen profiles were shown to be (nearly) uniform for all drying methods applied. This would imply similar dissolution rates. However, the dissolution rate is not only a function of the API profile but also of the pellet micro-structure. The drying method greatly affected the pellet micro-structure (porosity) for pellets dried *via* lyophilization. As the porosity was increased after lyophilization, more ibuprofen was released over 6 h in phosphate buffer. Additionally, the pore size may affect the dissolution behavior (44,45), since for porous, non-disintegrating pellets, the dissolution medium needs to enter the pores using capillary forces prior to the API dissolution. The median pore diameter (Table IV) was similar for all D and L. Thus, in this case, differences in the pellet porosity caused differences in the *in vitro* dissolution profiles. For FB, the porosity was similar to D, but the median pore diameter increased (Table IV). Therefore, the dissolution rate was faster. An increase in the pore diameter contributes to faster

Table V. Results for the Drug Release Mechanism over the First 6 h

	Zero order	Higuchi	Korsmeyer–Peppas	
Formulation	R^2	R^2	R^2	n
D1	0.9625	0.9963	0.9963	0.4940
D2	0.9529	0.9991	0.9994	0.5214
FB1	0.8540	0.9740	0.9931	0.3653
FB2	0.8667	0.9792	0.9928	0.3858
L1	0.8970	0.9891	0.9980	0.3967
L2	0.9259	0.9973	0.9988	0.4593

Regardless of the drying technique, ibuprofen was released *via* a diffusion-based mechanism
n release exponent

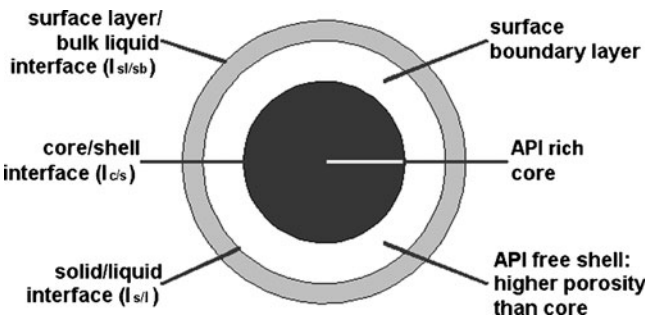

Fig. 9. Shrinking core model to explain the dissolution mechanism. During dissolution, an API-free shell and an API-rich core are formed. Solute API molecules diffuse from the core through the shell and the boundary layer into the bulk liquid

drug dissolution (45). In this case, differences in the pore diameter caused differences in the *in vitro* dissolution profiles. Obviously, the variations in the pellet density of FB1 and FB2 did not influence the release behavior, which implies that closed pores did not alter the overall release profile.

All graphs were best described by the Korsmeyer–Peppas model (Eq. 6; Table V). According to this model, the pellets released the API *via* a diffusion-based mechanism, as the calculated values for n were between 0.40 and 0.52. The release exponent n of the Korsmeyer–Peppas approach highlights the API release mechanism. For spheres, the value of 0.43 indicates pure Fickian diffusion, and the value of 0.85 indicates Case II transport (zero-order release). Values in between suggest the superposition of these two phenomena. A good correlation to the square root of time (Higuchi) model (Eq. 5) further supports a diffusion-controlled mechanism based on Fick's law. In summary, it can be concluded from the fitting data that the drug dissolution was mainly governed by diffusion for all methods of the pellet preparation, which is expected for this type of matrix material.

Since calcium stearate is hardly soluble in aqueous systems (dissolution medium), it can be assumed that only ibuprofen dissolved during the dissolution tests. Calcium stearate, however, remained solid. As the dissolution medium dissolved ibuprofen first from the pellet surface and progressively from regions close to the surface, an ibuprofen-free solid phase was formed on the outer part of the pellets leaving a gradually shrinking core, which contained the API (Fig. 9). The porosity of the ibuprofen-free shell was thus increased in comparison to the API-rich core. Considering the surface boundary layer near the pellet surface and the diffusion-based release mechanism, the dissolution can be explained using the shrinking core model. Dissolution occurred in three steps after the dissolution medium entered the pellet pores: (a) diffusion of solute ibuprofen molecules from the core/shell interface (Fig. 9, $I_{c/s}$) through the shell to the solid/liquid interface (Fig. 9, $I_{s/l}$), (b) diffusion of solute ibuprofen from $I_{s/l}$ through the surface boundary layer to the surface layer/bulk liquid interface (Fig. 9, $I_{sl/bl}$), and (c) diffusion of solute ibuprofen molecules from $I_{sl/bl}$ to the bulk liquid. Diffusion of the dissolved ibuprofen may be controlled by the surface boundary layer and/or by the ibuprofen-free shell. However, in the present study, the boundary layer transport was not rate-limiting due to the vigorous stirring in the dissolution apparatus.

CONCLUSIONS

This study clearly demonstrated that drying greatly affects the micro-structure of calcium stearate/ibuprofen pellets. Lyophilization resulted in the highest pellet porosity. The porosity after desiccation and fluid-bed drying was similar, but the median pore diameter was increased after fluid-bed drying. The differences in the pellet porosity were due to the shrinkage of CaSt, with drying conditions determining the extent of shrinkage. The spatial ibuprofen distribution within the pellets, however, was not affected by the drying conditions under investigation and was homogeneous for all batches. The dissolution characteristics depended upon the pellet micro-structure. The dissolution rate was the lowest after desiccation. Fluid-bed drying yielded in increased dissolution rates due to increased pore diameters. Pellets dried *via* lyophilization showed higher dissolution rates due to increased porosities. These results should be taken into account with regard to the manufacturing of drugs/dosage forms and, especially, the drying process.

ACKNOWLEDGMENTS

We would like to acknowledge Werba-Chem, Vienna, Austria for providing calcium stearate and G.L. Pharma, Lannach, Austria for providing ibuprofen. Furthermore, we thank Boril Chernev of Felmi, Graz, Austria for his assistance with the Raman mapping; Bettina Bauer of the University of Graz, Austria for the HPLC measurements; and Michael Piller, RCPE GmbH, Graz, Austria for help with the image analyses.

REFERENCES

1. Pérez JP, Rabisková M. Influence of the drying technique on theophylline pellets prepared by extrusion-spheronization. Int J Pharm. 2002;242(1–2):349–51.
2. Kleinebudde P. Shrinking and swelling properties of pellets containing microcrystalline cellulose and low substituted hydroxypropylcellulose: I. Shrinking properties. Int J Pharm. 1994;109(3):209–19.
3. Berggren J, Alderborn G. Drying behaviour of two sets of microcrystalline cellulose pellets. Int J Pharm. 2001;219(1–2):113–26.
4. Song B, Rough SL, Wilson DI. Effects of drying technique on extrusion-spheronisation granules and tablet properties. Int J Pharm. 2007;332(1–2):38–44.
5. Wlosnewski JC, Kumpugdee-Vollrath M, Sriamornsak P. Effect of drying technique and disintegrant on physical properties and drug release behavior of microcrystalline cellulose-based pellets prepared by extrusion/spheronization. Chem Eng Res Des. 2010;88(1):100–8.
6. Balaxi M, Nikolakakis I, Kachrimanis K, Malamataris S. Combined effects of wetting, drying, and microcrystalline cellulose type on the mechanical strength and disintegration of pellets. J Pharm Sci. 2009;98(2):676–89.
7. Gómez-Carracedo A, Souto C, Martinez-Pacheco R, Concheiro A, Gómez-Amoza JL. Incidence of drying on microstructure and drug release profiles from tablets of MCC–lactose–Carbopol® and MCC–dicalcium phosphate–Carbopol® pellets. Eur J Pharm Biopharm. 2008;69(2):675–85.
8. Berggren J, Alderborn G. Effect of drying rate on porosity and tabletting behaviour of cellulose pellets. Int J Pharm. 2001;227(1–2):81–96.
9. Bashaiwoldu AB, Podczeck F, Newton JM. A study on the effect of drying techniques on the mechanical properties of pellets and compacted pellets. Eur J Pharm Biopharm. 2004;21(2–3):119–29.
10. Balaxi M, Nikolakakis I, Malamataris S. Preparation of porous microcrystalline cellulose pellets by freeze-drying: effects of wetting liquid and initial freezing conditions. J Pharm Sci. 2009;99(4):2104–13.
11. Gómez-Carracedo A, Souto C, Martínez-Pacheco R, Concheiro A, Gómez-Amoza JL. Microstructural and drug release properties of oven-dried and of slowly or fast frozen freeze-dried MCC-Carbopol® pellets. Eur J Pharm Biopharm. 2007;67(1):236–45.
12. Murray T, Rough SL, Wilson DI. The effect of drying technique on tablets formed from extrusion–spheronization granules. Chem Eng Res Des. 2007;85(7):996–1004.
13. Bashaiwoldu AB, Podczeck F, Newton JM. The application of non-contact laser profilometry to the determination of permanent structural change induced by compaction of pellets: II. Pellets dried by different techniques. Eur J Pharm Biopharm. 2004;22(1):55–61.
14. Sousa JJ, Sousa A, Podczeck F, Newton JM. Influence of process conditions on drug release from pellets. Int J Pharm. 1996;144(2):159–69.

15. Lutchman D, Dangor CM, Perumal D. Formulation of rate-modulating pellets for the release of ibuprofen: an extrusion/spheronization process. J Microencapsul. 2005;22(6):643–59.
16. Dyer AM, Khan KA, Aulton ME. Effect of the drying method on the mechanical and drug release properties of pellets prepared by extrusion–spheronization. Drug Dev Ind Pharm. 1994;20(20):3045–68.
17. Ansari MA, Stepanek F. Design of granule structure: computational methods and experimental realization. AIChE J. 2006;52 (11):3762–74.
18. Ansari MA, Stepanek F. The evolution of microstructure in three-component granulation and its effect on dissolution. Part Sci Technol. 2008;26:55–66.
19. Lekhal A, Glasser BJ, Khinast JG. Impact of drying on the catalyst profile in supported impregnation catalysts. Chem Eng Sci. 2001;56(15):4473–87.
20. Liu X, Khinast JG, Glasser BJ. A parametric investigation of impregnation and drying of supported catalysts. Chem Eng Sci. 2008;63(18):4517–30.
21. Warren JW, Price JC. Drug migration during drying of tablet granulations I: Effect of particle size of major diluent. J Pharm Sci. 1977;66(10):1406–9.
22. Warren JW, Price JC. Drug migration during drying of tablet granulations II: Effect of binder solution viscosity and drying temperature. J Pharm Sci. 1977;66(10):1409–12.
23. Kiekens F, Zelko R, Remon JP. A comparison of the inter- and intragranular drug migration in tray- and freeze-dried granules and compacts. Pharm Dev Technol. 1999;4(3):415–20.
24. Kiekens F, Zelko R, Remon JP. Influence of drying temperature and granulation liquid viscosity on the inter- and intragranular drug migration in tray-dried granules and compacts. Pharm Dev Technol. 2000;5(1):131–7.
25. Kapsidou T, Nikolakakis I, Malamataris S. Agglomeration state and migration of drugs in wet granulations during drying. Int J Pharm. 2001;227(1–2):97–112.
26. Roblegg E, Ulbing S, Zeissmann S, Zimmer A. Development of lipophilic calcium stearate pellets using ibuprofen as model drug. Eur J Pharm Biopharm. 2010;75(1):56–62.
27. Gowen AA, O'Donnell CP, Cullen PJ, Bell SEJ. Recent applications of chemical Imaging to pharmaceutical process monitoring and quality control. Eur J Pharm Biopharm. 2008;69(1):10–22.
28. van de Water LGA, Bergwerff JA, Leliveld G, Weckhuysen BM, de Jong KP. Insights into the preparation of supported catalysts: a spatially resolved Raman and UV–vis spectroscopic study into the drying process of CoMo/γ-Al2O3 catalyst bodies. J Phys Chem B. 2005;109(30):14513–22.
29. Shipway PH, Hutchings IM. Fracture of brittle spheres under compression and impact loading. I. Elastic stress distributions. Phil Mag A. 1993;67(6):1389–404.
30. Ravisankar S, Vasudevan M, Gandhimathi M, Suresh B. Reversed-phase HPLC method for the estimation of acetaminophen, ibuprofen and chlorzoxazone in formulations. Talanta. 1998;46(6):1577–81.
31. ICH. Harmonised tripartite guideline: validation of analytical procedures: text and methodology Q2 (R1). Geneva: ICH; 2005.
32. Bragg WL. The diffraction of short electromagnetic waves by a crystal. Proc Camb Phil Soc. 1913;17:43–57.
33. Glatter O, Kratky O, editors. Small angle X-ray scattering. New York: Academic; 1982.
34. Rough SL, Wilson DI. Extrudate fracture and spheronisation of microcrystalline cellulose pastes. J Mater Sci. 2005;40(16):4199–219.
35. Yoshinari T, Forbes RT, York P, Kawashima Y. The improved compaction properties of mannitol after a moisture-induced polymorphic transition. Int J Pharm. 2003;258(1–2):121–31.
36. Airaksinen S, Karjalainen M, Räsänen E, Rantanen J, Yliruusi J. Comparison of the effects of two drying methods on polymorphism of theophylline. Int J Pharm. 2004;276(1–2):129–41.
37. Shah KR, Hussain MA, Hubert M, Farag Badawy SI. Form conversion of anhydrous lactose during wet granulation and its effect on compactibility. Int J Pharm. 2008;357(1–2):228–34.
38. Tantry JS, Tank J, Suryanarayanan R. Processing-induced phase transitions of theophylline-implications on the dissolution of theophylline tablets. J Pharm Sci. 2007;96(5):1434–44.
39. Römer M, Heinämäki J, Miroshnyk I, Sandler N, Rantanen J, Yliruusi J. Phase transformations of erythromycin A dihydrate during pelletisation and drying. Eur J Pharm Biopharm. 2007;67 (1):246–52.
40. Manrique J, Martinez F. Solubility of ibuprofen in some ethanol +water cosolvent mixtures at several temperatures. Lat Am J Pharm. 2007;26(3):344–54.
41. Jbilou M, Ettabia A, Guyot-Hermann A-M, Guyot J-C. Ibuprofen agglomerates preparation by phase separation. Drug Dev Ind Pharm. 1999;25(3):297–305.
42. Bika DG, Gentzler M, Michaels JN. Mechanical properties of agglomerates. Powder Tech. 2001;117(1–2):98–112.
43. Verkoeijen D, Meesters GMH, Vercoulen PHW, Scarlett B. Determining granule strength as a function of moisture content. Powder Tech. 2002;124(3):195–200.
44. Mehta KA, Kislalioglu MS, Phuapradit W, Malick AW, Shah NH. Effect of formulation and process variables on porosity parameters and release rates from a multi unit erosion matrix of a poorly soluble drug. J Contr Release. 2000;63(1–2):201–11.
45. Costa FO, Pais AACC, Sousa JJS. Analysis of formulation effects in the dissolution of ibuprofen pellets. Int J Pharm. 2004;270(1–2):9–19.